Sequential Acquisition and Processing of Perfusion and Diffusion MRI Data for a Porcine Stroke Model

Matthew A. Neimark, Andrew F. Laine, Erwin Lin, Stephen Dashnaw, and John Pile-Spellman

Abstract— **An automated data processing pipeline, designed for handling a large throughput of sequentially acquired MRI brain data, is described. The system takes as input multiple diffusion weighted (DWI) and perfusion weighted imaging (PWI) volumes acquired at different temporal points, automatically segments and registers them, and ultimately outputs a database used to track various perfusion and diffusion parameters through time at individual brain voxels. This pipeline has been utilized to successfully process two pig brains from an induced stroke experiment.**

I. Introduction

Diffusion and Perfusion weighted MRI imaging are now widely utilized for the clinical evaluation of ischemic stroke patients [1]. Perfusion Weighted MRI Diffusion weighted MRI (PWI) is effective at mapping out the location and extent of an ischemic insult [2] whereas Diffusion Weighted MRI is used to calculate the apparent diffusion coefficient (ADC) of water which spatially and quantitatively describes the extent of damage incurred by the decrease of blood flow [3].

There has been an expectation that this technology could be used to develop sensitive clinical algorithms to determine treatment procedures for patients based on their MRI readings [4]. This hope has largely not come to fruition due to the inability to develop a quantitative model based on MRI that accurately predicts the temporal progression of stroke [5].

The development of such a model is hampered by many factors including the uncertainty in the correlation between ADC and reversible or irreversible ischemic damage [6], limits to the accuracy of standard quantitative perfusion measurements [7], and the generally complex and qualitative nature of stroke models which already exist [8].

Probably one of the biggest obstacles toward the development of a quantitative stroke model is the lack of experimental data with sufficient temporal resolution to not only describe baseline and end points, but also measure at intermediate times during development of an infarct. Previous attempts to create statistical predictive stroke models based on MRI measurements have utilized data well outside the three hour time limit for which stroke is primarily thought to evolve [9].

Manuscript received May 2, 2005.

M. A. Neimark and A. F. Laine are with the Department of Biomedical Engineering, Columbia University, New York, NY 10027 USA (phone: 212-854-5996; fax: 212-854-5995; e-mail: Laine@ columbia.edu).

E. Lin, S. Dashnaw, and J. Pile-Spellman are with the Department of Radiology, Columbia University, New York, NY 10032 USA (e-mail: jp59@ columbia.edu).

Further, previous developments of mathematical stroke models did not compare their results to experimental data [10, 11]. This resulted in a potentially useful model that could not be effectively evaluated. These models often incorporated parameters that could not be easily accessed by MRI or other physical measurements.

To circumvent these issues, a series of porcine stroke experiments was performed in which DWI and PWI were acquired immediately after vessel occlusion, and continued to be acquired at a high sampling rate during stroke development. This high temporal resolution allows for effective monitoring during the entire course of the stroke.

However, given the large amount of data collected over this rather long acquisition period, and the potential for the animal to move during the study, it was necessary to devise a scheme to correct for movement of the animal so that stationary brain voxels could be monitored over the entire course of the study. Furthermore, given the large amount of data in the studies and the potential for human error, it is also necessary that this scheme be automated. Thus an automated segmentation and registration data pipeline has been implemented which efficiently processes raw input data and outputs a voxel-based database in which the temporal evolution of perfusion and diffusion parameters in individual brain voxels can be analyzed over the course of the experiment. This database provides a rich basis from which a mathematical stroke model can be effectively tested.

This study demonstrates the feasibility of sequentially acquiring DWI and PWI MRI data and subsequently sending the data through a segmentation/registration pipeline which efficiently and automatically creates an output voxel-based database.

II. Methods

A. Experiment

This study utilized two female 18-25 kg domestic pigs (Animal Biotech Industries, Danboro, PA) and was approved by the institutional care and use committee at Columbia University. Animals were anesthetized with isoflurane while cardiac and respiratory parameters were carefully monitored to ensure homeostatic stability.

Transfemoral catheterization was performed under MR guidance using active tracking [12] to physically obstruct the left and right carotid arteries and left subclavian artery.

All imaging was performed with a 1.5 T MR imaging system (TwinSpeed; GE Medical Systems, Milwaukee, Wis.) and a neurovascular array coil. DWI imaging was performed using gradient-echo EPI using two *b* values per

image [3] (b=0 and 1000 seconds/mm^2). This imaging utilized the following parameters: TR=10,000 ms, TE=76.4 ms, matrix=128 x 128, field of view (FOV)=16 cm, flip angle=90˚ and slice thickness 2.5 mm (no interspacing).

PWI imaging utilized dynamic susceptibility imaging using interarterial bolus injection (administered through a pigtail catheter in the ascending aorta). The bolus (50% gadolinium mixed with saline) was administered with a power injector at a rate of 2 cc/sec (6 cc total volume) followed by saline flush 2 cc/sec (6 cc total volume). 34 PWI volumes were acquired in sequence with a sampling rate of 1.25 Hz. PWI imaging was performed using gradient-echo EPI utilizing the following parameters: TR=1250 ms, TE=39 ms, matrix=64 x 64, field of view (FOV)=16 cm, flip angle=90˚, and slice thickness 2.5 mm (no interspacing).

B. Segmentation

All data was collected in DICOM format. Data post-processing software was written in MATLAB and "C". Data segmentation was performed for both DWI and PWI volumes independently. For the DWI images, segmentation was performed separately for the b=0 volumes and b=1000 volumes, although they were acquired simultaneously. For the perfusion, the volumes could theoretically be averaged across all time points for a single perfusion study. However, the gadolinium injection attenuates signal during passage through the brain. Therefore, a principal component analysis was performed using the time series measurements of all voxels in the volume. The onset of the bolus injection for the entire brain could be easily detected using the component corresponding to the largest eigenvalue. All volumes prior to this time point were thus averaged for segmentation.

Segmentation for both DWI and PWI was performed using a level-sets algorithm designed to minimize the Mumford-Shah functional [13]. The algorithm was run for 250 iterations where convergence was observed. A morphological segmentation algorithm was then performed to remove non-connected components to the central brain structure.

C. Registration

Co-registration of DWI to DWI volumes, and PWI to PWI volumes was first performed. This was accomplished through two stages. In the first stage, the volumes were rotationally aligned without correcting for translational shifts. All volumes are first recentered within the acquisition window by calculating their center of mass. This minimizes volume cut-off in the process of rotating the volumes during rotation of the volumes. The actual registration was then performed by minimizing

$$F(\theta,\phi,\varphi)=\left|\left|\Im\{u_1(x,y,z)\}\right|-\left|\Im\left\{R_T\left[u_2(x,y,z)\right]_{\theta,\phi,\varphi}\right\}\right|, \quad (1)$$

where u_1 is the reference image, u_2 is the pre-registered image, $R_T[\bullet]_{\theta,\phi,\varphi}$ is the rotational transformation across the three Euler angles θ, ϕ, and φ, and $\Im\{\bullet\}$ is the three-dimensional Fourier transform. This method is based on the principle that the magnitude of the Fourier transform is invariant to translational shifts. Minimization of $F(\theta,\phi,\varphi)$ is performed by the gradient descent method [14] (function *fminunc* in MATLAB). In addition, the rotational registration was performed using a multiresolution framework: The algorithm was first performed after successive levels of one-half downsampling (after first low-pass filtering as a means of anti-aliasing) whereby angle parameter estimates from downsampled volumes are used as initial guesses to the next higher level downsampled volumes until the registration for non-downsampled volumes is performed.

The second stage of the volume registration involves correcting the translational shifts between the registered and reference volumes. This was performed through the phase-correlation method [15] in three dimensions. Briefly, after calculating $u_2'=R_T[u_2]_{\theta,\phi,\varphi}$, u_2' is a translated version of u_1. i.e. $u_2'(x,y,z)=u_1(x-x_0,y-y_0,z-z_0)$. The cross power spectrum of $u_1(x,y,z)$ and $u_2'(x,y,z)$ is in theory an exponential. This is represented by the following equation:

$$\mathrm{X}_{PS}(u_1,u_2')=\frac{\Im\{u_1\}\Im\{u_2'\}^*}{\left|\Im\{u_1\}\Im\{u_1\}^*\right|}=e^{-i(fx_0+gy_0+hz_0)}. \quad (2)$$

where f, g, and h are the spatial frequencies. In order to determine x_0, y_0, and z_0, the inverse Fourier transform of X_{PS} is calculated:

$$\Im^{-1}\{\mathrm{X}_{PS}(u_1,u_2')\}=\delta(x_0,y_0,z_0). \quad (3)$$

x_0, y_0, and z_0 can then be identified by spatial location of the impulse.

The reference volumes (inter-registration of PWI and DWI data) used for these registrations were determined by estimating the major axes of inertia of each volume. The volumes whose inertial axis was most parallel to the coordinate axes were used as the reference.

To register the PWI to the DWI data, co-registered PWI and DWI volumes were averaged across acquisitions, and the mutual information algorithm [16] was used to register the averaged PWI volume to the averaged DWI volume.

The mutual information algorithm is similar to the rotational registration algorithm in that the gradient descent method is used to minimize a function describing the quality of registration between the transformed pre-registered volume and reference volume (in the case of rotational registration it is the difference between Fourier Transform magnitudes as expressed by (1)). It also uses a multiresolution scheme (similar to rotational registration).

However, in the case of mutual information, six parameters (as opposed to three in the rotational registration case) are optimized as the translational shift parameters must

also be corrected through gradient descent, as the mutual information scheme does not support phase-correlation as described by (2).

D. Calculation of ADC

ADC maps were calculated through logistic regression of the signal intensity of parallel DWI images [17] acquired with different *b* values. Since we have two parallel DWI acquisitions (*b*=0 and *b*=1000), this reduces to the formula:

$$ADC(x,y,z) = \frac{\ln[S_0(x,y,z)] - \ln[S_{1000}(x,y,z)]}{1000\ {}^{S}/_{mm^2}} \quad (4)$$

E. Calculation of Blood Perfusion Parameters

For PWI, the relation between MRI signal and gadolinium contrast concentration for a voxel is [18]

$$S(t) = S_0 e^{-kC_c(t)TE} \quad (5)$$

where S_0 is the baseline signal, $C_c(t)$ is the contrast concentration, k is a normalization factor, $S(t)$ is the measured signal, and TE is the time to echo in the MRI sequence. Thus, calculation of contrast concentration can be performed by

$$C_c(t) = \frac{\ln[S_0] - \ln[S(t)]}{k \cdot TE}. \quad (6)$$

Three parameters were calculated, relative cerebral blood volume (rCBV), relative cerebral blood flow (rCBF), and mean transit time (MTT).

The value rCBV was calculated as the integral under the perfusion curve [18]:

$$rCBV = \int_{onset}^{offset} C_c(t)dt \quad (7)$$

A differentiation-filter based algorithm was used to calculate the bolus onset and offset times for this integral.

The value rCBF was calculated as the peak of the first derivative of $C_c(t)$ [19]:

$$rCBF = \max\left[\frac{dC_c(t)}{dt}\right]. \quad (8)$$

We defined MTT as the width of the bolus peak at half maximum:

$$t_1 = \underset{t>0}{\arg\min}\left[C_c(t) > {}^{1}/_{2}\max[C_c(t)]\right]$$
$$t_2 = \underset{t>t_1}{\arg\max}\left[C_c(t) > {}^{1}/_{2}\max[C_c(t)]\right] \quad (9)$$
$$MTT = t_2 - t_1$$

F. Mathematical Phantoms

In order to comprehensively test the segmentation/registration procedure, a mathematical phantom study was conducted whereby a single DWI (*b*=1000) volume was randomly rotated by all three Euler angles (<=±10˚), randomly shifted along all three axes (<=±10 mm), and corrupted with white Gaussian noise (5-35% of average signal intensity). This random transformation (rotation+translation+noise) was performed 20 times for each phantom test, and the segmentation/registration algorithm was employed in an attempt to reconstruct the known angle and translation. The results are displayed in Table II.

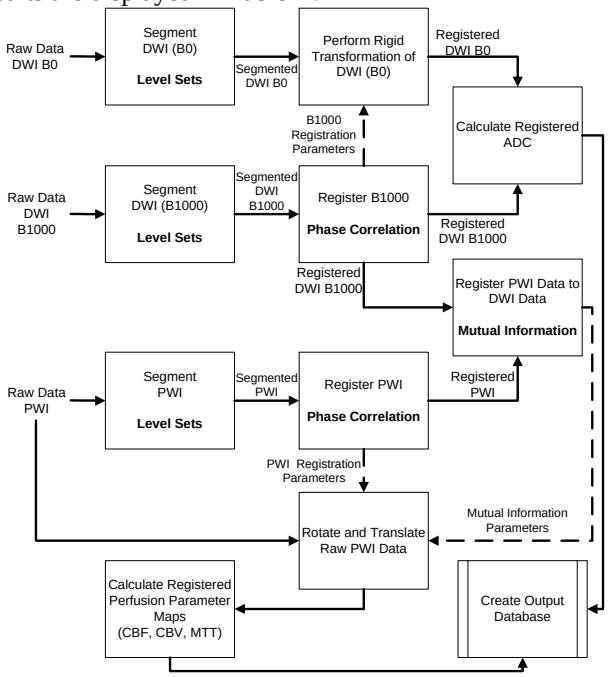

Fig. 1. Data pipeline including segmentation, registration, and post processing steps to produce a quantitative voxel database.

III. Results

A. Studies

A summary of the two pig experiments is shown in Table I. Vessels were successfully occluded (as confirmed by MRI Angiography) in both pigs. For Pig 1, there were approximately 2 DWI acquisitions per hour and 1 PWI acquisition for hour while for Pig 2, there were approximately 4.75 DWI acquisitions per hour and 1.67 PWI acquisitions per hour. The bulk of the acquisitions occurred during and after the vessel occlusions.

B. Phantoms

Phantom study results are demonstrated in Table II. The experiments showed that angular errors (although not transitional errors) accumulate slightly with increasing noise, but are kept within reasonable limits even for normal experimental noise levels (15-25%). Slice encoding transitional errors are larger and axial angle errors smaller due to higher sampling in the axial planes (0.0625 mm vs. 2.5 mm)

TABLE I
SUMMARY OF EXPERIMENTS

Pig	# of DWI Acquisitions	# of PWI Acquisitions	Time of Exam	Time of Stroke
1	21	11	10 hrs. 30 minutes	5 hrs. 52 minutes
2	34	12	7 hrs. 12 minutes	5 hrs. 40 minutes

C. Temporal Evolution of Stroke

Fig. 2 demonstrates the time evolution of the stroke taken from a region of interest in Pig 1. The perfusion course is shown to correspond very closely with the ADC. It is also interesting to note that the ADC levels off to a stable steady state (~66% of baseline) in the last four hours.

TABLE II
MATHEMATICAL PHANTOM EXPERIMENTS

Noise	A (mm)	B (mm)	C (mm)	D	E	F
5 %	0.76	0.83	1.13	0.25˚	0.34˚	0.072˚
15%	0.69	0.62	1.03	0.26˚	0.23˚	0.064˚
25 %	0.76	0.86	1.14	0.22˚	0.33˚	0.093˚
35%	0.69	0.65	1.10	0.37˚	0.40˚	0.11˚

Registration shift errors in the (A) MRI phase encoding direction, (B) MRI gradient encoding direction, (C) MRI slice encoding direction. Registration rotational errors in the (D) sagittal plane, (E) coronal plane, and (F) axial plane.

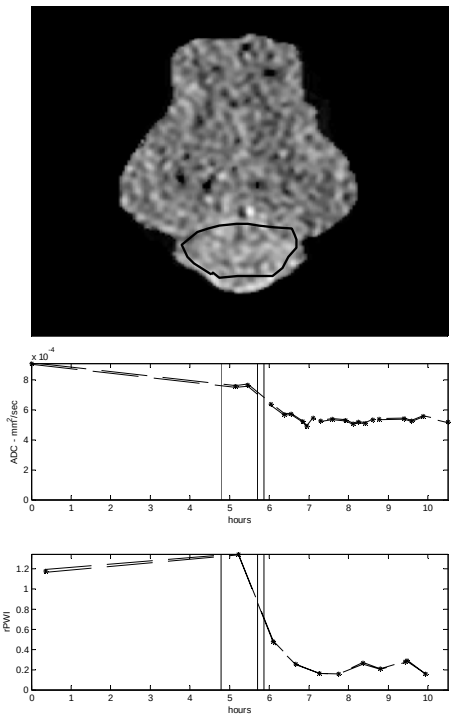

Fig. 2. Time evolution of stroke during experiment for ROI in DWI *b*=1000 image (top) for Pig 1. Vertical bars represent occlusion times. Asterices represent acquistition points for the particular volume. Dashed lines represent standard error bounds.

IV. CONCLUSIONS

This study demonstrates the feasibility and effectiveness of a comprehensive segmentation/registration pipeline for high data output porcine stroke experiments. This culminates in the ability to monitor diffusion and perfusion parameters in a localized region of brain as shown in Fig. 2. It is a goal to use this scheme as a platform for testing a mathematical stroke model against experimental data. As shown in Fig. 2 the high temporal resolution of the data produced by these experiments is sufficient for such comparisons. Future efforts will strive to make this process real-time to provide feedback and monitoring of the experiment during the interventional part of the procedure.

REFERENCES

[1] J. V. Guadagno, G. A. Donnan, R. Markus, J. H. Gillard, and J. C. Baron, "Imaging the ischaemic penumbra," *Current Opinion in Neurology*, vol. 17, pp. 61-7, 2004.

[2] S. L. Keir and J. M. Wardlaw, "Systematic review of diffusion and perfusion imaging in acute ischemic stroke," *Stroke*, vol. 31, pp. 2723-31, 2000.

[3] P. W. Schaefer, P. E. Grant, and R. G. Gonzalez, "Diffusion-weighted MR imaging of the brain," *Radiology*, vol. 217, pp. 331-45, 2000.

[4] G. Schlaug, A. Benfield, A. E. Baird, B. Siewert, K. O. Lovblad, R. A. Parker, R. R. Edelman, and S. Warach, "The ischemic penumbra: operationally defined by diffusion and perfusion MRI," *Neurology*, vol. 53, pp. 1528-37, 1999.

[5] S. Warach, "Tissue viability thresholds in acute stroke: the 4-factor model.[comment]," *Stroke*, vol. 32, pp. 2460-1, 2001.

[6] J. Fiehler, M. Foth, T. Kucinski, R. Knab, M. von Bezold, C. Weiller, H. Zeumer, and J. Rother, "Severe ADC decreases do not predict irreversible tissue damage in humans," *Stroke*, vol. 33, pp. 79-86, 2002.

[7] K. A. Rempp, G. Brix, F. Wenz, C. R. Becker, F. Guckel, and W. J. Lorenz, "Quantification of regional cerebral blood flow and volume with dynamic susceptibility contrast-enhanced MR imaging," *Radiology*, vol. 193, pp. 637-41, 1994.

[8] E. H. Lo, T. Dalkara, and M. A. Moskowitz, "Mechanisms, challenges and opportunities in stroke," *Nature Reviews Neuroscience*, vol. 4, pp. 399-415, 2003.

[9] O. Wu, W. J. Koroshetz, L. Ostergaard, F. S. Buonanno, W. A. Copen, R. G. Gonzalez, G. Rordorf, B. R. Rosen, L. H. Schwamm, R. M. Weisskoff, and A. G. Sorensen, "Predicting tissue outcome in acute human cerebral ischemia using combined diffusion- and perfusion-weighted MR imaging," *Stroke*, vol. 32, pp. 933-42, 2001.

[10] E. Ruppin, E. Ofer, J. A. Reggia, K. Revett, and S. Goodall, "Pathogenic mechanisms in ischemic damage: a computational study," *Computers in Biology & Medicine*, vol. 29, pp. 39-59, 1999.

[11] V. Duval, S. Chabaud, P. Girard, M. Cucherat, M. Hommel, and J. P. Boissel, "Physiologically based model of acute ischemic stroke," *Journal of Cerebral Blood Flow & Metabolism*, vol. 22, pp. 1010-8, 2002.

[12] L. Feng, C. L. Dumoulin, S. Dashnaw, R. D. Darrow, R. Guhde, R. L. Delapaz, P. L. Bishop, and J. Pile-Spellman, "Transfemoral catheterization of carotid arteries with real-time MR imaging guidance in pigs," *Radiology*, vol. 234, pp. 551-7, 2005.

[13] T. F. Chan and L. A. Vese, "Active contours without edges," *IEEE Transactions on Image Processing*, vol. 10, pp. 266-77, 2001.

[14] R. Fletcher and M. J. D. Powell, "A rapidly convergent descent method for minimization," *Computer Journal*, vol. 6, pp. 163-8, 1963.

[15] C. D. Kuglin and D. C. Hines, "The phase correlation image alignment method," *Proceedings of the IEEE International Conference on Cybernetics and Society*, pp. 163-5, 1975.

[16] J. P. Pluim, J. B. Maintz, and M. A. Viergever, "Mutual-information-based registration of medical images: a survey," *IEEE Transactions on Medical Imaging*, vol. 22, pp. 986-1004, 2003.

[17] R. Luypaert, S. Boujraf, S. Sourbron, and M. Osteaux, "Diffusion and perfusion MRI: basic physics," *European Journal of Radiology*, vol. 38, pp. 19-27, 2001.

[18] L. Ostergaard, R. M. Weisskoff, D. A. Chesler, C. Gyldensted, and B. R. Rosen, "High resolution measurement of cerebral blood flow using intravascular tracer bolus passages. Part I: Mathematical approach and statistical analysis," *Magnetic Resonance in Medicine*, vol. 36, pp. 715-25, 1996.

[19] E. Klotz and M. Konig, "Perfusion measurements of the brain: using dynamic CT for the quantitative assessment of cerebral ischemia in acute stroke," *European Journal of Radiology*, vol. 30, pp. 170-84, 1999.